Geochemistry Geophysics Geosystems G3

Article
Volume 11, Number 5
11 May 2010
Q05003, doi:10.1029/2009GC002933
ISSN: 1525-2027

Published by AGU and the Geochemical Society

Lava deposition history in ODP Hole 1256D: Insights from log-based volcanostratigraphy

Masako Tominaga
Department of Oceanography, Texas A&M University, 3146 TAMU, College Station, Texas 77843-3146, USA

Now at Department of Geology and Geophysics, Woods Hole Oceanographic Institution, Woods Hole, Massachusetts 02543, USA (mtominaga@whoi.edu)

Susumu Umino
Department of Earth Sciences, Kanazawa University, Kakuma-machi, Kanazawa 920-1192, Japan

[1] A log-based volcanic stratigraphy of Ocean Drilling Program Hole 1256D provides a vertical cross-section view of in situ upper crust formed at the East Pacific Rise (EPR) with unprecedented resolution. This stratigraphy model comprises ten electrofacies, principally identified from formation microscanner images. In this study, we build a lava flow stratigraphy model for the extrusive section in Hole 1256D by correlating these electrofacies with observations of flow types from the modern EPR, such as sheet flows and breccias, and pillow lavas and their distribution. The resulting flow stratigraphy model for the Hole 1256D extrusive section represents the first realization of detailed in situ EPR upper oceanic crust construction processes that have been detected only indirectly from remote geophysical data. We correlated the flow stratigraphy model with surface geology observed from the southern EPR (14°S) by *Shinkai 6500* dives in order to obtain the relationship between lava flow types and ridge axis-ridge slope morphology. This dive information was also used to give a spatial-time reference frame for modeling lava deposition history in Hole 1256D. In reconstructing the lava deposition history, we interpreted that the origins of the ~100 m thick intervals with abundant pillow lavas in Hole 1256D are within the axial slope where pillow lavas were observed during the *Shinkai 6500* dives and previous EPR surveys. This correlation could constrain the lava deposition history in Hole 1256D crust. Using the lateral scale of ridge axis–ridge slope topography from the *Shinkai 6500* observations and assuming the paleospreading rate was constant, 50% of the extrusive rocks in Hole 1256D crust were formed within ~2000 m of the ridge axis, whereas nearly all of the remaining extrusive section was formed within ~3000 m of the ridge axis. These results are consistent with the upper crustal construction model previously suggested by seismic studies.

Components: 10,100 words, 8 figures, 2 tables.

Keywords: Ocean Drilling Program; Hole 1256D; volcanostratigraphy; East Pacific Rise; wireline logging.

Index Terms: 3036 Marine Geology and Geophysics: Ocean drilling; 3045 Marine Geology and Geophysics: Seafloor morphology, geology, and geophysics; 3075 Marine Geology and Geophysics: Submarine tectonics and volcanism.

Received 29 October 2009; **Revised** 23 February 2010; **Accepted** 8 March 2010; **Published** 11 May 2010.

Copyright 2010 by the American Geophysical Union

Tominaga, M., and S. Umino (2010), Lava deposition history in ODP Hole 1256D: Insights from log-based volcanostratigraphy, *Geochem. Geophys. Geosyst.*, *11*, Q05003, doi:10.1029/2009GC002933.

1. Introduction

[2] Magmatic and volcanic processes at mid-ocean ridges form ocean crust that covers nearly 60% of Earth's surface. The architecture in the extrusive part of the oceanic crust has important influences on hydrothermal circulation and hydration of the lithosphere. Many terrestrial and marine surveys have attempted to describe the architecture accurately by investigating the upper crustal construction processes [e.g., *Moores and Vine*, 1971; *Casey et al.*, 1981; *Alt et al.*, 1996; *Fornari et al.*, 2004]. In terrestrial settings, the investigation of the Troodos and Oman ophiolites have provided the architecture on various scales, which is thought to be analogous to modern-day intermediate to fast spreading mid-ocean ridge upper crust [*Moores and Vine*, 1971; *Moores and Jackson*, 1974; *Coleman*, 1977; *Rautenschlein*, 1987; *Bednarz and Schumincke*, 1989; *Alt*, 1994; *Nicolas*, 1995; *Dilek et al.*, 1998]. In marine settings, numerous submersible surveys, seismic experiments, and several basement drilling expeditions have provided the structure and the surficial volcanic processes of the fast spreading crust [*Alt et al.*, 1993, 1996; *Karson et al.*, 2002; *Fornari et al.*, 1998, 2004; *Christeson et al.*, 2007]. In spite of these efforts, how upper ocean crust construction processes take place with a time-distance reference frame has only been described at the scale of geophysical investigations and bathymetry data [e.g., *Schouten and Denham*, 1979; *Hooft et al.*, 1996; *Christeson et al.*, 2007; *Escartín et al.*, 2007; *Soule et al.*, 2009], and virtually no detailed architectural information is considered in these models. This is because of differences in sampling resolution between those geophysical data and geologic observations.

[3] Ocean Drilling Program (ODP) Hole 1256D was the first successful drilled hole to recover a complete section of intact upper oceanic EPR crust [*Wilson et al.*, 2003; *Teagle et al.*, 2006]. Whereas the coring suffered from low recovery rates (volcanic section average 37%) and biased rock types in the extrusive section, wireline logs provide quasi-continuous in situ physical property data with excellent quality. In particular, multidimensional wireline tool strings, such as the formation microscanner (FMS) and the ultrasonic borehole imager (UBI), provided high-resolution images of the in situ borehole wall, enabling the reconstruction of an upper crustal architecture model with unprecedented resolution ("volcanostratigraphy model" [*Tominaga et al.*, 2009]). This volcanostratigraphic model makes it possible to identify end-member lava flow types in the extrusive section, such as massive flows, pillows, and breccias, and qualifies their distribution downhole.

[4] In general, we can assume that the lava flows observed at the lower part of the volcanic section are older than flows above and were deposited close to the ridge axis. With this as a premise, we can assume that the lava sequence in Hole 1256D represents a history from the first lava eruption and deposition at the paleo–East Pacific Rise (EPR) ridge axis to the last off-axis lava eruption and deposition. By integrating this in situ lava sequence in Hole 1256D with previously observed surface geology and remote geophysical measurements at the modern EPR, we should be able to suggest an upper crustal construction process model with unprecedented time-distance reference frame. In this study, we introduce the translation of the extrusive section of Hole 1256D log-based stratigraphy into a lava flow stratigraphy and propose the first realization of fine-scale in situ upper oceanic crust constructional processes from a single drilled hole.

2. Geological Background

2.1. East Pacific Rise Lava Flows

[5] Numerous submarine geological surveys have been carried out to characterize detailed surface morphology and lava flow types around fast spreading EPR axial regions. These data were obtained by multibeam (and microbeam) bathymetry, side-scan sonar, and remotely operated vehicle (ROV) and autonomous underwater vehicle (AUV), and submersible dive data [e.g., *Wright et al.*, 1995; *Embley et al.*, 1998; *Kurras et al.*, 2000; *Scheirer et al.*, 2000; *White et al.*, 2000; *Bazin et al.*, 2001; *White et al.*, 2002; *Cormier et al.*, 2003; *Fornari et al.*, 2004; *Soule et al.*, 2005, 2007; *Stakes et al.*, 2006; *Escartín et al.*, 2007; *Ferrini et al.*, 2007; *Soule et al.*, 2009; *White et al.*, 2009]. These observations indicate that

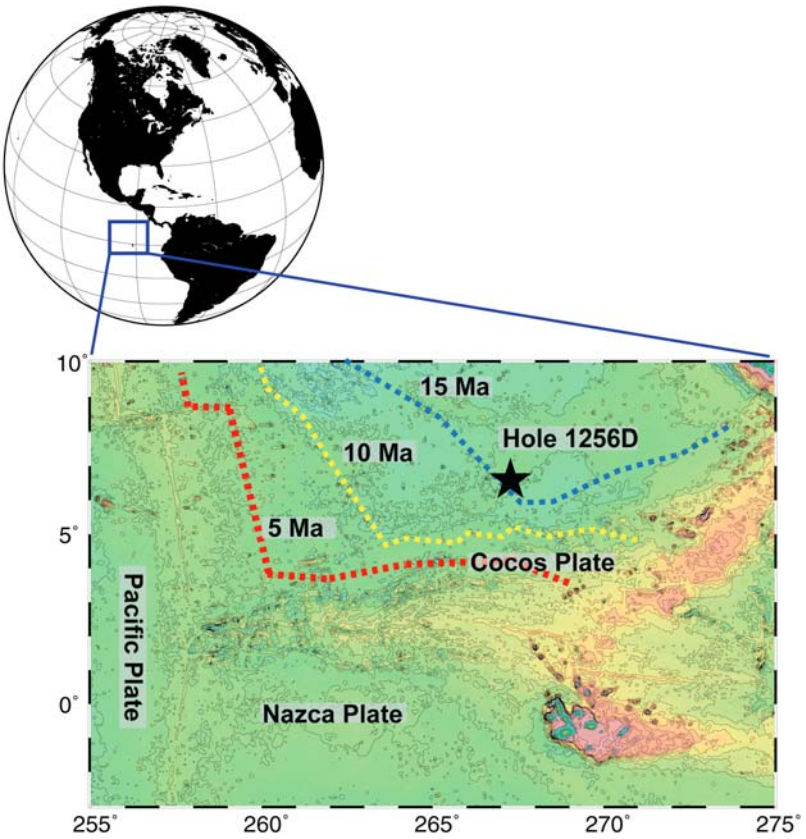

Figure 1. Location map and bathymetry map of the Cocos-Nazca-Pacific region and location of ODP/IODP Hole 1256D. Red and blue dashed lines indicate 10 and 15 Ma isochrons, respectively. Bathymetry data were obtained from *Smith and Sandwell* [1997].

the evolution of EPR submarine lava flows is analogous to the down-flow transition of subaqueous lava flows observed on the Hawaiian Islands, where lava flows evolve from proximal sheet flows, to lobates, to pillows [e.g., *Soule et al.*, 2004; *Fornari et al.*, 2004]. Both lobate and sheet flows are ubiquitous flow types from the EPR axial eruptions and are distributed uniformly along and across the axial regions [e.g., *Kurras et al.*, 2000; *White et al.*, 2000]. Lavas that form these flows may also have traveled substantial distances from the ridge axis very long distance from the axis (approximately a few thousands of meters) via lava tubes and channels [e.g., *Soule et al.*, 2005]. Pillow lavas are, on the other hand, a rather minor flow type and are more localized and distributed near fissures and fractures on the EPR axis. Pillow lavas also appear at distant locations from the axis and flow fronts [e.g., *Kurras et al.*, 2000; *Soule et al.*, 2005] and accumulate as pillow mounds at the average of ~2300 m from the axis on the typical EPR seafloor [*Soule et al.*, 2009] or within overlapping spreading center basins at the EPR discontinuities [*White et al.*, 2009].

2.2. ODP Hole 1256D Drilling Results

[6] ODP Hole 1256D (6°44.2′N, 91°56.1′W) is located in the Guatemala Basin on the northeastern flank of the EPR (Figure 1). Surface magnetic anomalies suggest that the crust is 15 Ma and accreted at superfast spreading rates (full ~220 km/Myr) [*Wilson et al.*, 2003]. The total drilled sequence is 1507.1 m beneath the seafloor (mbsf) with coring or curatorial depth (hereafter mbsf-C) and is composed of a 754 m extrusive lava section, a 403.4 m dike complex (including 58.3 m of granoblastic dikes), 54 and 24 m gabbro sections embedded in 24 m of dike screen, and a few meters of basaltic dikes at the bottom of the hole [*Teagle et al.*, 2006]. The uppermost crust is made up of a single >74 m thick ponded lava flow. This thick lava correlates with a 32 m thick massive lava cored in the nearby Hole 1256C indicating

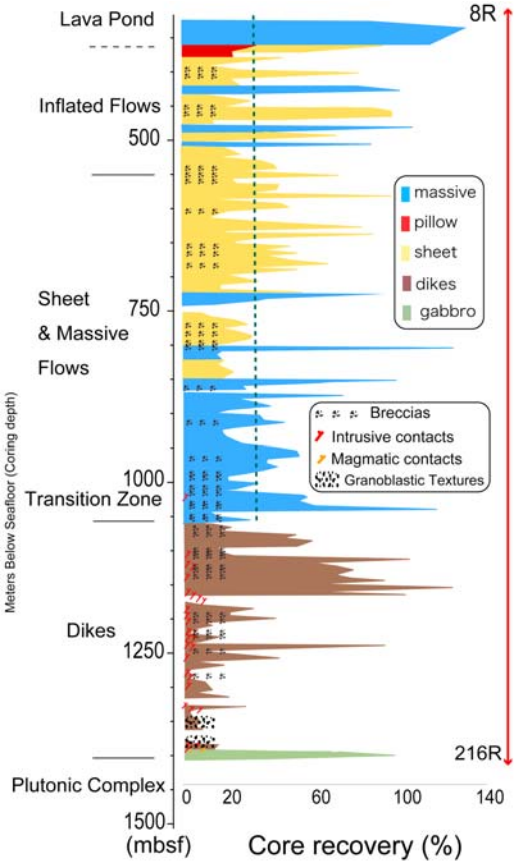

Figure 2. Summary of shipboard stratigraphy in Hole 1256D, the interval of which corresponds to the logged interval. The red arrow on the right indicates logged interval that corresponds from Cores 8R to 216R. The core recovery rates (horizontal axis in %) and recovered core types (colored) are shown. The dotted line indicates the average core recovery rate (32%).

significant basement topography at the time of eruption. By analogy with observations of the modern EPR [*Macdonald et al.*, 1996] and the need for significant topography to pond such a thickness of lava, this massive flow is interpreted to have emplaced 5 to 10 km off axis [*Wilson et al.*, 2003]. Structural analysis of the basal crust of the ponded flow indicates that it was erupted from an off-axial vent nearby [*Crispini et al.*, 2006]. The lavas directly underlying the ponded flow display rare subvertical hyaloclastite-filled inflation structures, indicative of eruption onto a near horizontal surface [e.g., *Umino et al.*, 2002], and are interpreted to have also solidified off axis. Sheet flows with subordinate massive (>3 m thick) flows make up the bulk of the extrusive section (533.9 to 1004.1 mbsf-C). Subvertical igneous contacts, commonly brecciated and mineralized associating with dike intrusions, are abundant throughout the lower part of the extrusive formations. Both the isolated dikes in the extrusive rocks and the distances between two dike margins in the sheeted dike complex are typically ~0.5 ± 0.8 m and are dipping ~79° with a dip direction of 53° (away from the ridge axis) [*Tominaga et al.*, 2009]. The lower 60 m of the dike complex shows recrystallized, distinctive granoblastic textures that indicate contact metamorphism by gabbro intrusions [*Koepke et al.*, 2007]. Two gabbro intervals have chilled margins against the host granoblastic dikes [*Teagle et al.*, 2006].

[7] Nearly all of the drilled sequence has normal mid-ocean ridge basalt (MORB) composition and is similar to, but slightly depleted compared to, modern EPR basalts [*Teagle et al.*, 2006]. Basaltic flows and dikes show a wide range of magmatic fractionation, and primitive and evolved compositions are closely juxtaposed [*Wilson et al.*, 2003]. The lava sequence is much less hydrothermally altered than other drilled basement sites (e.g., Hole 504B) [*Alt et al.*, 1996].

3. Methods: Logging Operations in Hole 1256D Upper Oceanic Crust

[8] The downhole lithostratigraphy provides the basic foundation for our understanding of the architecture of drilled section of oceanic crust. It has been challenging, however, to build an accurate lithostratigraphy model due to low recovery rates (~30%) and the scarcity of long, continuous recovered core pieces through basement drilling. Shipboard stratigraphy is, hence, subjective due to biased recovery of rock types, fractures, and alteration styles (e.g., loss of highly altered breccia materials and fracture fillings). Consequently, the shipboard volcanostratigraphy may lead one to erroneous classifications of lithologic types, interpretations of crustal construction processes, and calculations of chemical fluxes from seawater-rock alteration (Figure 2).

[9] As an alternative to such shipboard stratigraphy, *Tominaga et al.* [2009] reconstructed a qualitative volcanostratigraphy model of Hole 1256D by analyzing electrofacies collected during formation microscanner (FMS) and ultrasonic borehole imager (UBI) runs (Figure 3). The FMS tool string measures electric current returns that are sensitive to the porosity structure and cation exchange capacity of the formation [*Pezard*, 1990]. The FMS tool uses four orthogonal pads each with 16 sensor

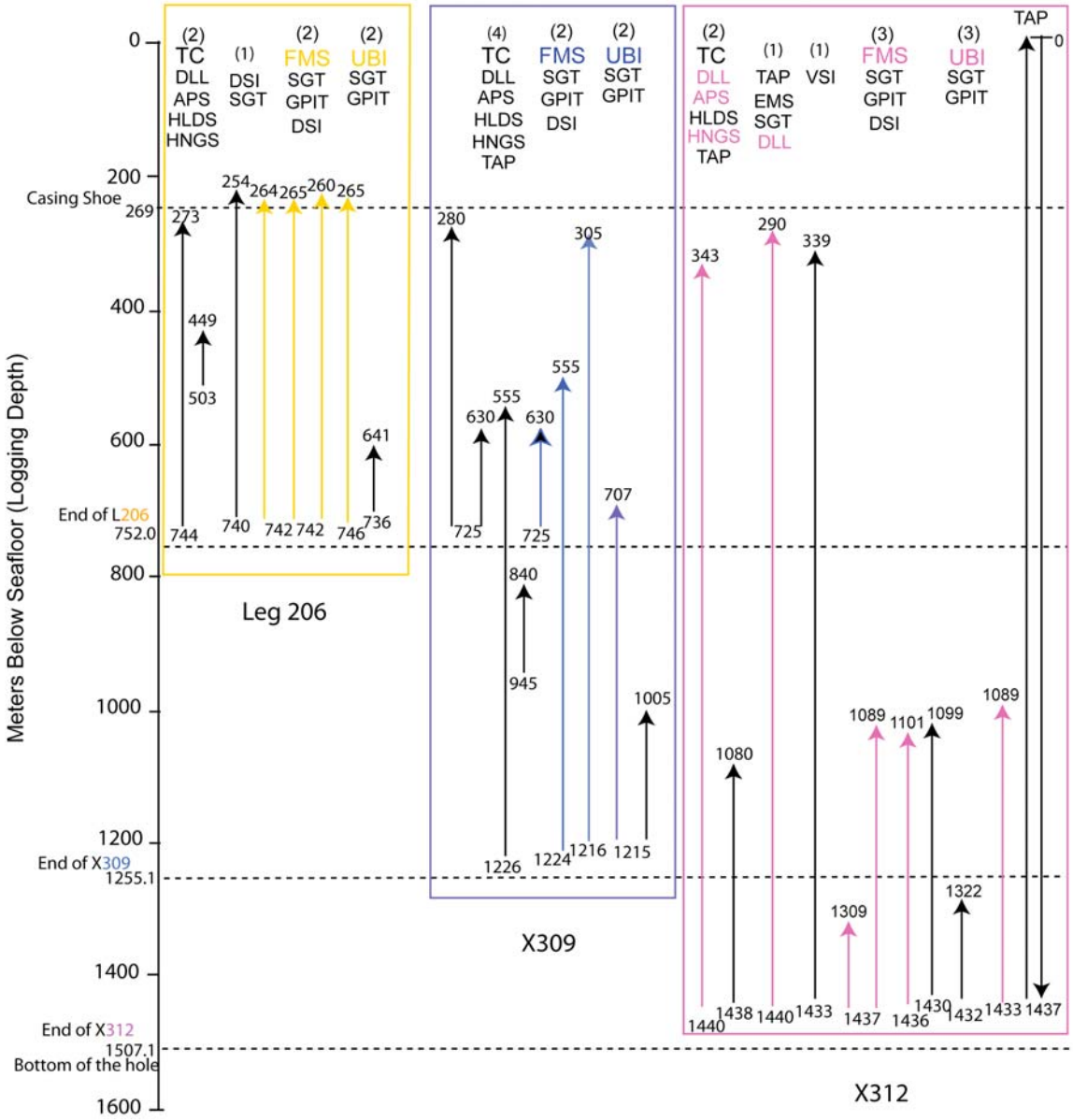

Figure 3. Summary of Leg 206 (yellow) and Expeditions 309 (blue) and 312 (pink) logging operations. Colored lines and letters indicate wireline logs that were used in this study. The top and bottom of the logging depth are indicated (mbsf-L). Numbers in parentheses (1–4) indicate the number of passes with tools indicated below the number. TC, triple combo; HNGS, hostile environment gamma ray sonde; APS, accelerator porosity sonde; HLDS, hostile environmental lithodensity sonde; DLL, dual laterolog; TAP, temperature acceleration pressure tool; SGT, scintillation gamma ray tool; DSI, dipole sonic imager; GPIT, general purpose inclinometer tool; FMS, formation microscanner; UBI, ultrasonic borehole imager; VSI, versatile seismic imager; EMS, environmental mechanical sonde.

buttons to collect the electric current returns, covering the borehole wall (e.g., up to 40% with four orthogonal pads in 8 in. borehole) with a high resolution (~0.002 m) of resistivity readings. The resulting FMS data provide high-resolution resistivity contrast of the borehole wall and exhibit the detailed architecture of the borehole wall, i.e., the electrofacies. The UBI tool string measures the acoustic reflections from the borehole wall with 360° coverage, and provides a visualization of the borehole wall reflectivity as two-dimensional images with a sampling resolution of ~0.15 m. The FMS and UBI in situ physical property measurements essentially provide "scanned images" of the borehole wall that are of essential for determining the morphology of the penetrated basement for-

Table 1. Parameters in Each Lithofacies for Qualitative Volcanostratigraphy[a]

Electrofacies		Primary Parameters			
Number	Name	LogLLD	LogLLS	NGR	FMS/UBI Criteria: Primary Morphology on FMS Images
1	massive flows	2.0 ± 0.3	2.0 ± 0.3	2.6 ± 0.8	>2 m thick, with almost no developed fractures resulting in featureless, homogeneous textures.
1a	massive off-axis ponded lava	1.9 ± 0.2	1.7 ± 0.2	2.6 ± 1.3	Homogeneous texture, subordinate fractures.
2	fractured massive flows	1.6 ± 0.2	1.6 ± 0.2	3.8 ± 1.3	Less homogeneous texture due to some fracture development, >2 m thick.
3	pillow lavas	1.6 ± 0.2	1.5 ± 0.2	4.4 ± 1.1	An oval to subround outline with radial fracture inside, associated with altered interpillow materials showing high conductivity.
4	thin flows or thick pillows	1.6 ± 0.2	1.6 ± 0.2	4.3 ± 1.3	Similar to homogeneous texture in massive flows disturbed by distinctive flow boundaries or horizontal fractures, <2 m thick.
5	fragmented flows	1.4 ± 0.3	1.4 ± 0.3	5.7 ± 2.8	Brecciated and develop meshy fractures but individual blocks are only slightly displaced each other, thickness vary.
6	breccias	1.2 ± 0.3	1.0 ± 0.3	4.9 ± 2.0	Completely fragmented, no morphology preservation, the mixture of extremely fine high and low FMS conductivity patches.
7a	isolated dikes	1.8 ± 0.3	1.6 ± 0.4	2.3 ± 1.0	Distinguished by highly conductive, steep dip fractures, most likely representing intrusive contacts against the host extrusive rocks.
7	dikes in the sheeted dike complex	2.6 ± 0.6	2.3 ± 0.4	4.3 ± 1.3	Recognized by subparallel, subvertical fractures spaced ~0.6 m apart, indicating dike contacts.
8	gabbro	NA	NA	NA	(data only available from cores)

[a]LLD, dual laterolog deep penetration; LLS, dual laterolog shallow penetration; NGR, natural gamma ray counts; NA, data not available. Units for LogLLD and LogLLS are Ω m and for NGR are API counts. Primary parameters are calculated from wireline log during IODP Expedition 312.

mations. Both the FMS and UBI images are azimuthally oriented to the geographic reference frame using the general purpose inclinometer tool. The condition of Hole 1256D is considered "reliable" as there are a few significant washout intervals (>14 in.) in the upper part of the hole (348–403, 418–435, 450–473, 530–605, and 678–694 mbsf with logging depth, hereafter mbsf-L [*Teagle et al.*, 2006]). The multiple passes of the FMS in Hole 1256D through three drilling expeditions resulted in the FMS logging operation yielding greater than 40 to 60% lateral coverage (as high as 216°) over 65% of the logged interval. This level of lateral coverage is the best among any FMS data acquired in basement drill holes to date and allows us to reconstruct downhole lithostratigraphy with confidence. The interpretation of the FMS images was augmented by ultrasonic borehole imager data.

[10] Other physical property logs, including one-dimensional resistivity data (dual laterolog deep and shallow penetrations), natural gamma ray counts, lithodensity and porosity logs, compressional velocity, photoelectric effect factor, and recovered core data are available for the entire drilled extrusive section. We used these logs to complement the interpretation of the FMS images (Table 1). It should be noted that the names of these electrofacies are principally developed from morphologies observed in the FMS images (detailed descriptions of logging tool strings and data acquisition system are presented by *Tominaga et al.* [2009]).

4. Results

[11] The resulting FMS-based downhole stratigraphy provides a more accurate architecture of the igneous formations in Hole 1256D with a spatial image resolution of 0.1 m compared to conventional shipboard lithostratigraphy. For the extrusive section, a total of seven electrofacies are recognized. These are ponded lava, massive flow, fractured massive flow, pillows, thick pillows/thin flows, fractured flows, and breccias. The extrusive section is underlain by isolated dikes and dikes in the sheeted dike complex (Figure 4a) [*Tominaga et al.*, 2009]. The core-log integration based on the electrofacies analysis revealed that the discrepancy between two depth scales, mbsf-C and mbsf-L, are only a few meters in Hole 1256D [*Gilbert and Burke*, 2008; *Tominaga et al.*, 2009]. All the recovered cores have corresponding depth intervals and in situ electrofacies that were assumed from the electrofacies analysis [*Tominaga et al.*, 2009].

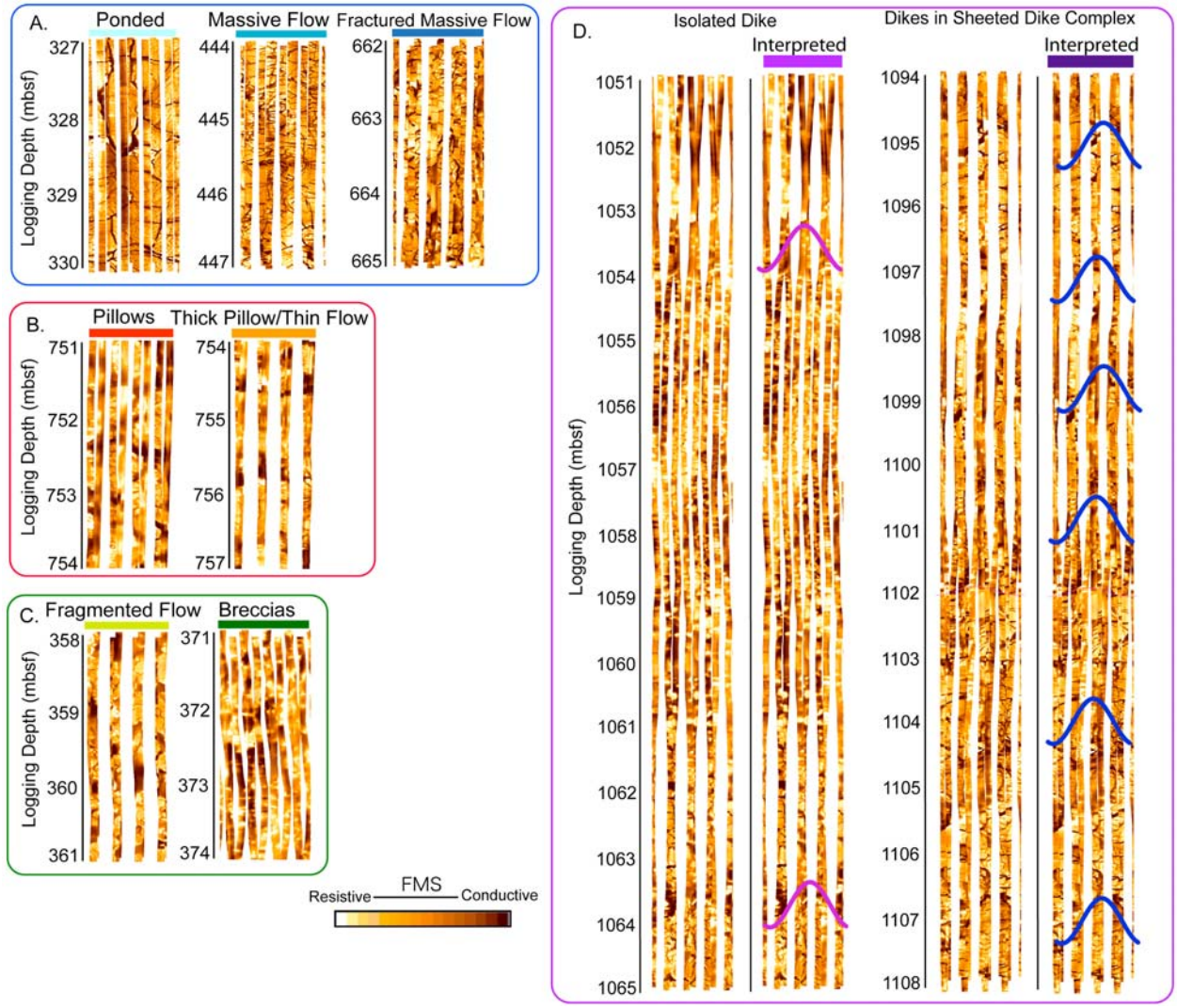

Figure 4. Examples from identified 10 electrofacies in Hole 1256D. (a) Massive flow family, (b) pillow family, (c) fractured flow family, and (d) FMS images for before and after the interpretation of dike margins. Sinusoids on isolated dikes and dikes show the locations of possible dike margins (details given by *Tominaga et al.* [2009]). Note that the electrofacies analyses were carried out by correlating the features observed in the FMS images with other physical property logs [*Tominaga et al.*, 2009].

4.1. Electrofacies Analysis in Hole 1256D Extrusive Section

[12] The electrofacies that exhibit massive flow origins (ponded lava, massive flow, and fractured massive flow) comprise 26% of the extrusive section [*Tominaga et al.*, 2009]. We identified massive flows as intervals of more than 2 m thick with a homogeneous texture on the FMS images. Irregularly spaced minor fractures with various orientations are common in these flows (Figure 4a). Although the characteristics of massive flows and ponded lava electrofacies are similar (Figure 4a), there are strong geological and geophysical criteria for their recognition as a distinctive subgroup [*Wilson et al.*, 2003] and relatively high core recovery rates give confidence in the shipboard descriptions. Fractured massive flows are another subgroup of massive flows that show a homogeneous texture with commonly rounded fractures apparent on the FMS images, but relatively high resistivity (Figure 4a). We assume that the fractured massive flows were originally massive flows that have been physically modified by fracturing or jointing.

[13] The electrofacies that exhibit pillow lava origins are the pillow lavas and thin flows/thick

pillows and are a subordinate portion of extrusive section (Figure 4b). We identified pillow lavas in the FMS images as rounded bodies with curved rims, radial fractures, downward drooping teardrop shapes, relatively highly conductive interstitial material, and irregular patches within the more massive interiors. Pillow lobe sizes measured from the FMS images range from a few tens centimeters to approximately 1 m in diameter. The thin flows/thick pillows electrofacies (average thickness 0.95 ± 0.4 m) are probably a part of the pillow lavas electrofacies. The thin flows/thick pillows electrofacies comprise ~1 m thick flows with relatively homogeneous textures in the FMS images, and common rounded boundaries (Figure 4b). It should be noted that the name of this electrofacies reflects the uncertainty of our determination of this type. A drill hole through the center of a ~1 m thick pillow lobe will have a similar wireline log responses to that of a ~1 m thick flow with distinctive flow boundaries on the top and bottom, because the curved rims of the pillow may not be intersected by the borehole or apparent on the FMS images. Hence, it is difficult to unequivocally determine solely from wireline logs whether this electrofacies type represents a thin sheet flow or relatively large pillow lobe [*Tominaga et al.*, 2009]. Additionally, we think that these pillow morphologies may be included in the fractured and fragmented flows and breccia electrofacies as pillow breccias [*Schmincke et al.*, 1978; *Yamagishi*, 1994; *Batiza and White*, 2000]. However, it is virtually impossible to distinguish small, fragmented pillow features within very complicated texture of those electrofacies.

[14] The electrofacies that exhibit highly fractured morphology are fragmented flows and breccias and these electrofacies comprise ~50% of the extrusive section (Figure 4c). Fragmented flows are the most abundant electrofacies in the volcanic sequence of Hole 1256D. The fractured flow electrofacies are thick intervals with the mesh fabric morphology, isolated by highly conductive, flow boundary zones or fractures. This mesh fabric morphology is much denser than fractured massive flows. The fragmented flows are thought to originate from massive flows although pervasive fracturing makes it difficult to discount other origins [*Tominaga et al.*, 2009].

[15] Breccias were identified for intervals with completely fragmented textures on the FMS images, in which the fragments of the original formations appear to be chaotically arranged. The highly fragmented texture of these formations makes it difficult to distinguish lithologic boundaries and conductive fractures. To date, the origins of the breccias observed in subaqueous lava eruptions at ocean spreading centers are classified into hyaloclastic, hydroclastic, spatter (agglutinate), and epiclastic. Recovered cores of hyaloclastite breccias consisting of glass clasts >8 cm across are recovered at 461 mbsf (Core 206-1256D-30R-1, 0–76 cm) and 597–599 mbsf (Core 206-1256D-51R-1, 84–150 cm and Core 206-1256D-51R-2, 0–142 cm). We presume that these hyaloclastite breccias are rubble formed by collapse of inflated lobate sheet flows or talus rubble in tension fissures and faults [e.g., *Engels et al.*, 2003]. Some brecciated zones occur along subvertical contacts that may be dike margins, in the FMS images (e.g., at 914 mbsf-L). Further investigation on core materials (Table 2) suggested that highly disrupted "mineralized volcanic breccia" at intervals 1027 to 1043 mbsf-C is most likely of hydroclastic origin formed by the interaction of water and hot, molten lava. These breccias consist of both angular and irregularly embayed lava clasts with or without glassy chilled margins set in a matrix of glass fragments. Clasts of lava recovered at 1050–1065 mbsf-C have intensely folded layers of alternating aphanitic and microcrystalline bands, which is akin to densely welded clasts of lava formed by moderate fountaining of lava. Lava fountaining is also inferred for the emplacement of the lowermost crust of the lava pond on top of the Hole 1256D [*Crispini et al.*, 2006].

[16] Isolated dikes occur within the volcanic section (<1064 mbsf-L) and present massive flow–like textures on the FMS images sandwiched between pairs of subvertical, high-conductivity bands with similar dips to the chilled margins observed in the underlying sheeted dike complex (Figure 4d). We identified 28 isolated dikes between 810–1064 mbsf-L. These isolated dikes observed from the FMS images are reminiscent of the narrow interfingered dikes rarely present in the recovered cores, although it is difficult to validate one-to-one correlations (e.g., interfingered dikes in Core 309-1256D-120R-1, 8–26 cm (1017.68–1017.94 mbsf-C) and isolated dikes observed at 1018 mbsf-L). The distance from one dike margin to the adjacent one is average of 2.9 m in the interval of 810–1064 mbsf-L. The average dip and dip directions of the contacts are ~79° ± 23° and 033 ± 67, respectively, calculated by using statistics of spherical coordinate system [*Fisher and Embleton*, 1987]. The characteristics of the isolated dikes are very similar to the dikes in the dike complex

Table 2. Reinvestigation of Breccias Recovered in Hole 1256D[a]

Expedition	Site	Hole	Core	Type	Section	Top	Bottom	Piece	Descriptions
309	1256	D	122	R	1	41	44	10a	Hyaloclastite.
309	1256	D	122	R	1	58	60	11	Round lithic clast in glassy hyaloclastic clasts.
309	1256	D	122	R	1	67	74	12	Hyaloclastite? Lithic clasts with chilled margin break into brittle pieces. Interstices filled with pyrite veins. Hydrofracturing?
309	1256	D	122	R	1	80	86	13a	Round lithic and glass clasts, indicative of fragmentation of plastic lava.
309	1256	D	122	R	1	106	111	15a	Round lithic and glass clasts, indicative of fragmentation of plastic lava.
309	1256	D	122	R	1	119	124	16	Plastic deformation of lithic clasts with chilled margin, which spall off into curved glass shards showing a fluidal fabric are truncated by brittle edges, but other clast margins are curved and irregularly engulfed, indicating hot fragmentation. Vent breccia?
309	1256	D	123	R	1	14	18	4	Glass clasts embedded in brittle lithic clasts.
309	1256	D	127	R	1	3	6	2	Massive lithic slab.
309	1256	D	128	R	1	6	12	2	Lithic slab showing ductile shear folding, suggestive of welded clasts of lava.

[a]These are observations on 4 mm slabs from IODP samples listed in Request 21873A&B_Tominaga_Umino (2009), Gulf Coast Core Repository.

(Figure 4d, where the average dip of the dikes in the dike complex is 76° ± 16° (N = 19) [*Tominaga et al.*, 2009]). Below 910 mbsf in Hole 1256D, isolated dikes are commonly associated with brecciated margins.

4.2. Lava Flow Stratigraphy for Hole 1256D Extrusive Section

[17] Next, we translated the electrofacies into end-member lava flow types observed at the EPR spreading regime. For our translation practice, we used two reference groups: (1) observations of the cross-sectional views of different styles of lava flows from ophiolites and submarine tectonic windows [e.g., *Yamagishi*, 1994; *Gillis and Sapp*, 1997; *Karson et al.*, 2002] and (2) the distribution of lava flow types in the vicinity of ridge axis at the modern EPR [e.g., *Ballard and Moore*, 1977; *Haymon et al.*, 1993; *Auzende et al.*, 1996; *Embley et al.*, 1998; *Kurras et al.*, 2000; *Batiza and White*, 2000; *White et al.*, 2000, 2002; *Sinton et al.*, 2002; *Umino et al.*, 2002; *Perfit et al.*, 2003; *Soule et al.*, 2005, 2007]. With these references in mind, we classified the electrofacies in the extrusive section of the downhole stratigraphy into pillows (pillow lavas and thin flow/thick flows), flows (massive flows and fractured massive flows), fractured (fragmented flows), and breccias. We decided to use only these four representatives so as not to overinterpret and mistranslate the electrofacies into actual lava flow types (Figure 5b).

[18] The resulting flow stratigraphy provides the first-order approximation of the lava flow sequence throughout the EPR basement that we will consider from the base to the top of the drilled section. Directly atop the dike complex (1064 mbsf-L), we observe ~100 m thick interval of flows and breccias, intruded by isolated fingering dikes. Around 950 mbsf-L, layers of breccias and flows become more abundant. This sequence is terminated by a sequence of thick flows around 850 mbsf-L. Pillow lavas are most abundant in one relatively restricted interval between 700 and 810 mbsf-L. The upper part of the hole (<700 mbsf-L) is composed of thick layers of flows, breccias, and the off-axis massive ponded lava (Figure 5b).

5. Discussion

[19] In the resulting flow stratigraphy in Hole 1256D, the 100 m thick pillow lava interval in the middle of the extrusive section is a striking feature because pillow morphologies are generally subordinate to other flows observed at the fast spreading modern EPR. If there is any robust correlation between the formations of pillow lavas and typical ridge morphology observed on the modern EPR, we should be able to link the downhole flow stratigraphy to the upper crustal construction processes. In sections 5.1–5.3, we propose a possible scenario to explain how pillows are localized and formed this thick interval in Hole 1256D crust and introduce a model of upper ocean construction process.

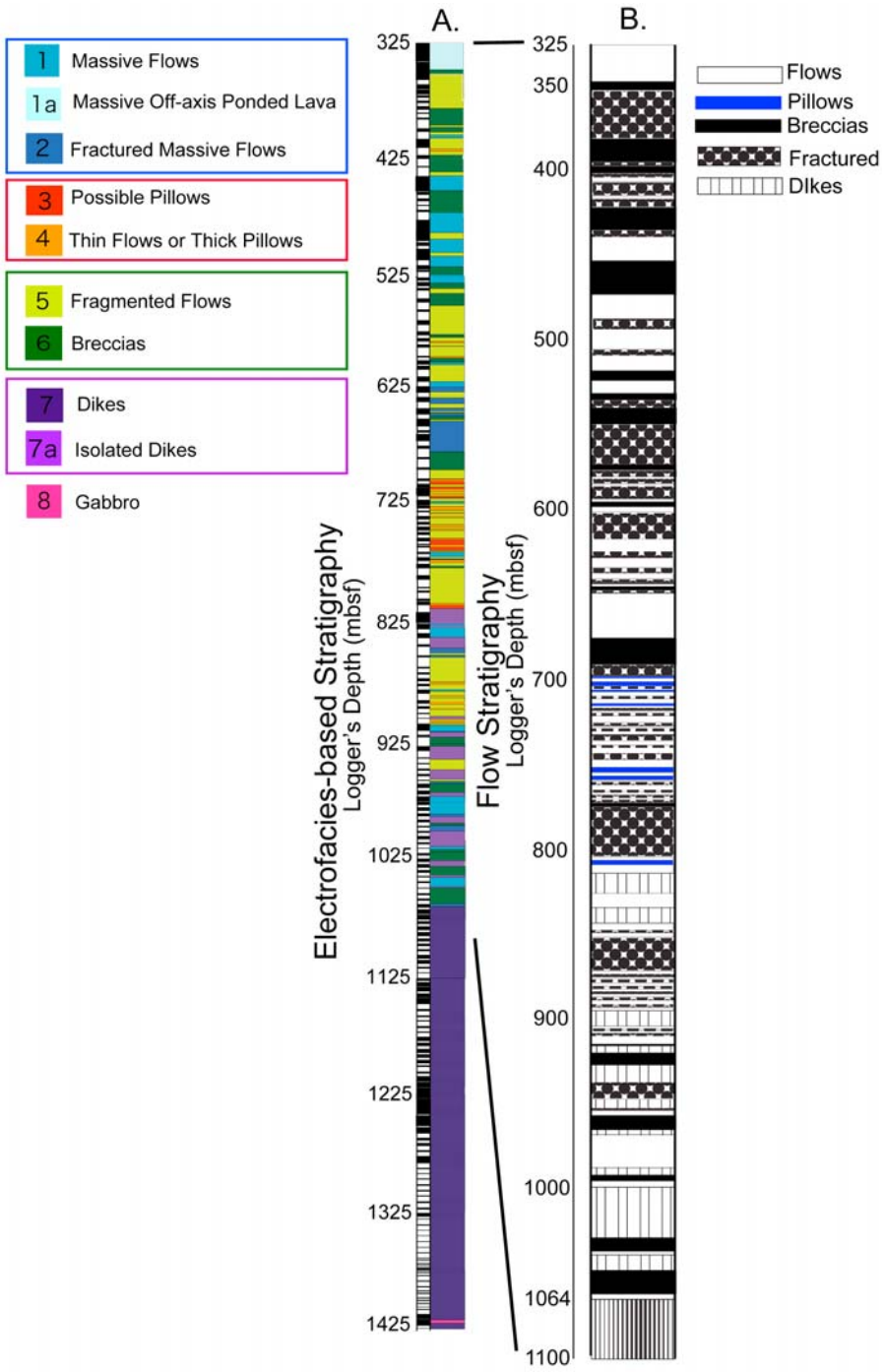

Figure 5. (a) Electrofacies-based stratigraphy and (b) flow stratigraphy for the volcanic section of Hole 1256D. We used logging depth (mbsf-L).

5.1. Formation of Pillow Lavas

[20] There is a widely held perception that the formation of pillow lavas depends on the spreading rate [*Bonatti and Harrison*, 1988]. However, pillow lavas are ubiquitously observed in all spreading environments, suggesting that spreading rate is only one of the controlling parameters that determine the abundance of pillows. What controls the formation of pillows as a consequence of axial eruptions is more likely to be a combination of effusion rate, changes in lava viscosity, and the slope of the preexisting topography [*Gregg and Fink*, 1995; *Griffiths*, 2000; *Kurras et al.*, 2000;

Umino et al., 2002; *Gregg and Smith*, 2003]. The former two parameters are strongly correlated to the rate of lava cooling during eruption and transportation. The slope angle enhances viscous/gravity flow of lavas [*Griffiths*, 2000]. The pillow lavas observed in the EPR are thereby interpreted to be a result of the combination of low effusion rate, high viscosity, and low slope angle [*Gregg and Fink*, 1995].

[21] Among these parameters, however, "low slope angle" is primarily based on dive observations focused on the EPR axial summit regions [e.g., *Kurras et al.*, 2000]. A series of description in previous studies suggest that the formation of pillows also occurs at the termination of lava flows (flow front) [e.g., *Soule et al.*, 2005] and as flows associated with changes in local topography, such as rise slopes [*Fornari et al.*, 1979; *Francheteau and Ballard*, 1983], faults and fissures near the ridge axis [*Sempéré and Macdonald*, 1986; *Auzende et al.*, 1996; *Bohnenstiehl and Carbotte*, 2001], and other subaqueous slopes [*Umino et al.*, 2000, 2002; *Gregg and Smith*, 2003]. Moreover, *White et al.* [2002] suggested that the EPR 9°N study area does not have extensive slope changes (typically, only <1° changes are observed) which can explain the distribution of lava morphology. The validity of "low" slope angle to form the pillows is rather questionable from these observations, and so we think there could be another factor that controls the wholesale lava deposition regime through upper crustal construction processes over the region from the ridge axis and ridge slope to the abyssal plain.

5.2. Dive Observation at Present-Day Fast Spreading Southern EPR Ridge

[22] One possible scenario to explain the formation of pillows with respect to regional topography is suggested from observations made on *Shinkai 6500* dives at the western flank of the EPR at 14°S during YK04–07 cruise by R/V *Yokosuka* in July 2004 [*Geshi et al.*, 2007; *Umino et al.*, 2008a, 2008b]. This part of the EPR has been known to have a half-spreading rates of 68 and 75 km/Myr to the west and east, respectively (Figure 6; see also Figure S1 (part A) in the auxiliary material).[1] The main objective of these dives was to investigate the difference in lava flow types and overall ridge topography in particular to slope angles. Two ~4000 m dive tracks were designed to cover the area from the ridge axis to the bottom of the axial slope (2640–2740 m water depth, ~2000 m from the ridge axis), where most of the upper oceanic crust is formed.

[23] Detailed lava flow types along dive tracks were described by S. Umino during dives and from dive videos. Slope angles were obtained from shipboard multibeam bathymetry data (Figure 6b; available at http://www.jamstec.go.jp/cruisedata/yokosuka/j/YK04-07.html). On the axial summit, where the surface angle ranges 0–5°, lobate sheet flows associated with subaqueous pahoehoe lobes and collapsed pits are the dominant lava deposition styles. Subaqueous pahoehoe lobes differ from pillow lobes in that they have lower ratios in thickness to width and lack corrugations on the surface, but have smooth and/or folded surface crust, suggesting a similar manner of lobe growth to subaerial equivalents [*Batiza and White*, 2000; *Umino et al.*, 2000, 2002]. These lava types indicate that this region is covered by flows of relatively low effusion rates [*Gregg and Chadwick*, 1996]. Fast moving sheet flows showing lineated or wrinkled surface crust, which are in part disrupted to form jumbled flows, are likely limited in channels on the bottom of collapse pits on lobate sheets. These fast moving sheet flows strongly suggest rapid drainage of lava either out of the inflating lobate sheets, which flow downslope toward the rise flank, or drain-back of lava into the eruptive fissure vent, leaving hollow lobate sheets with a thin roofed crust, which then collapses to form pits. The axial slope or faulted areas on axial summit (see track distance 3000 m in Figure S1 (parts B and C)), where the slope with >5° inclination (purple tick marks in Figure S1 (parts B and C)), are mostly covered by elongate pillows. Typical elongate pillows gradually change in shape into flattened elongate sheets and further into pahoehoe lobes that are connected to a wider, lobate sheet upstream as the slope gradually decreases toward the rise summit. Both pillow and sheet flows are nearly aphyric with only rare clinopyroxene microphenocrysts set in a glass matrix in the quenched flow surfaces. Therefore, equilibrium temperatures of clinopyroxene and glass following *Putirka* [1999] can be regarded as the lava temperature upon extrusion. Viscosities of lava at these temperatures were estimated by the method of *Giordano et al.* [2008]. Pahoehoe and lobate sheet flows and pillow lavas collected along both dive tracks show minimal differences in the estimated viscosity and temperatures ranging from 81 to 99 Pa s and 1181 to 1185°C, which are essentially nonunique from one to the

[1] Auxiliary materials are available in the HTML. doi:10.1029/2009GC002933.

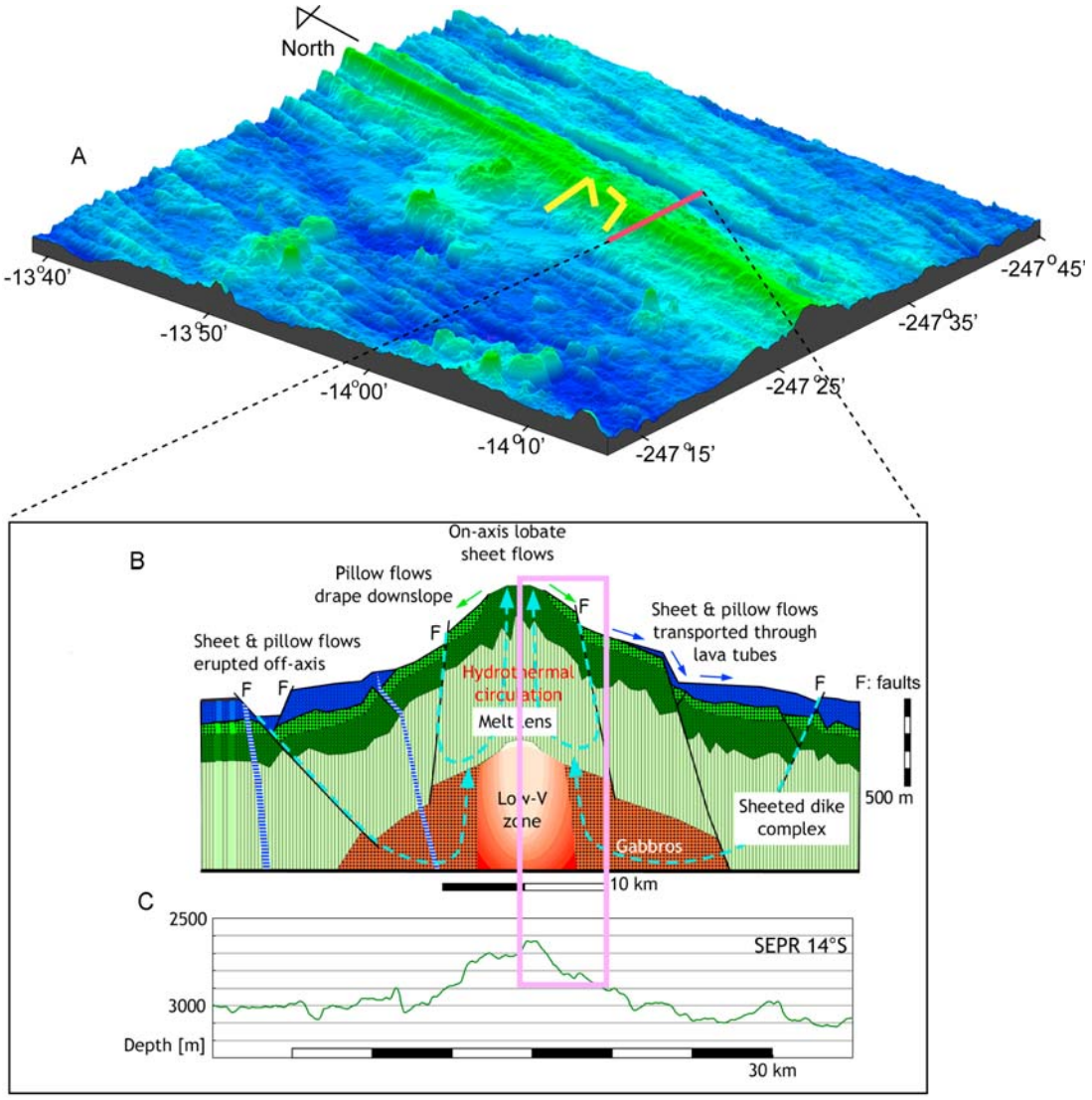

Figure 6. (a) Multibeam bathymetry of southern EPR (14°S) and (b and c) schematic plot of the cross section of the EPR. Yellow lines show *Shinkai 6500* dive tracks (see detailed track lines in Figure S1 (part A)). Multibeam bathymetry data are available at http://www.jamstec.go.jp/cruisedata/yokosuka/j/index.html. Schematic diagram of cross section of EPR 14°S (Figure 6b) with actual bathymetry data (Figure 6c). The bathymetry data are extracted from the multibeam data in Figure 6b. Pink box drawn over the middle of the diagram shows the region from ridge axis, ridge slope, and abyssal seafloor.

other, indicating that the viscosity is not the parameter responsible for a change in lava flow type [*Umino et al.*, 2008a, 2008b] (Figure S2). Instead, the observation suggests that the slope angle of >5° could be a threshold for the formation of pillow lavas in the EPR 14°S setting. This threshold is also applicable to subaqueous flows from Hawaii where lobate-pahoehoe flows dominate on subhorizontal basement, but on slopes are exclusively overlain by elongate pillows [*Umino et al.*, 2002; *Gregg and Smith*, 2003].

[24] The relationship between the ridge-scale morphology and lava flow types observed during these *Shinkai 6500* dives and the reexamination of previous studies suggests that the significant factors that determine lava flow types are a combination of underlying morphology, the kinetic energy of the lava flow front at the axial summit region, and the slope angle of local topography. Our scenario for the formation of pillow lavas during a low to moderate effusion rate eruption at a fast spreading regime is described as follows: low

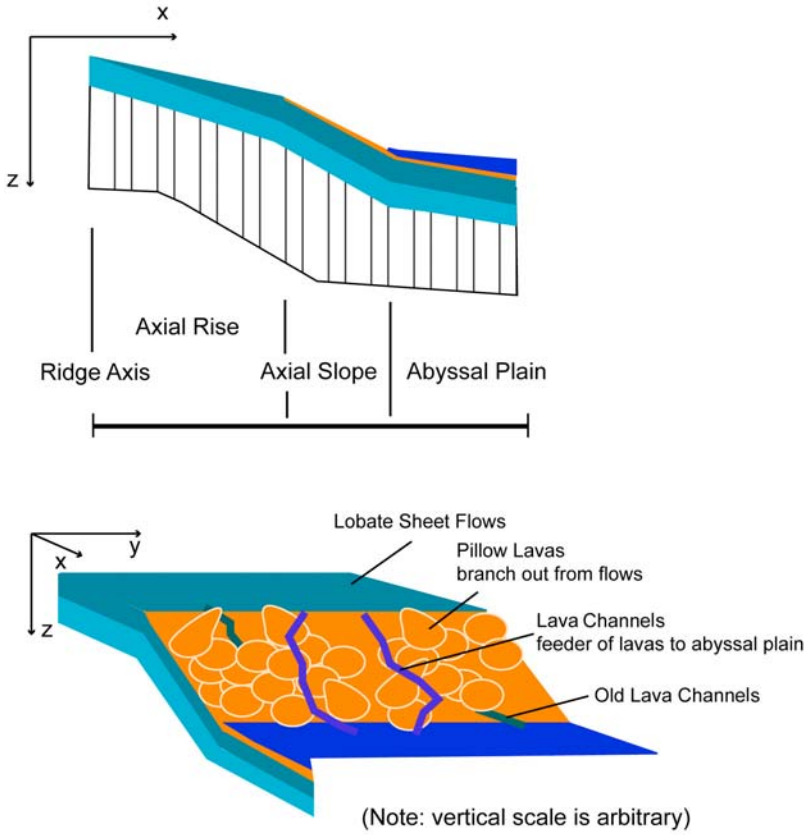

Figure 7. Schematic plot of the pillow lava formations on the axial slope.

to moderately extruding lava over a subhorizontal axial summit form slowly advancing pahoehoe flow lobes, which coalesce to form wider, inflating lobate sheets with hummocky topography. As the pahoehoe lobes, ahead of main lobate sheets, approach the steepening edge of the summit region, they turn into flat and elongate sheets downslope and then into elongate pillows on slopes. Rapid drainage of a mass of lava within lobate sheets is expected to occur when the front of coalesced lobate sheets approaches the edge of the rise summit. The outpouring the lava onto steepening slopes takes place. A part of the outpouring lava may travel even farther off axis regions via lava channels [*Fornari*, 1986; *Soule et al.*, 2005; *Escartín et al.*, 2007] (blue color streams in Figure 7).

[25] Further observations are needed to generalize the *Shinkai 6500* observations. For example, recent observations on the EPR 9°25′N–9°58′N seafloor suggest that pillow mounds are common at the average distance of 2300 m from the ridge axis, the formation of which might be taken place at the ridge axis by low–effusion rate eruptions. This constructional volcanic mounds may be the origin of the thick pillow interval in Hole 1256D [e.g., *Soule et al.*, 2009]. However, the vertical extent of these pillow mounds as well as the frequency of the low-effusion eruptions at the fast spreading EPR 9°N crust are not well described. Thus, we prefer to conclude that the observations at the EPR 14°S has a closer spreading condition to the crust of Hole 1256D, where the magma supply is sufficient to make frequent high-effusion eruptions and superfast spread seafloor with a narrow axial trough, and smooth axial summit topography without a caldera. Thus, if the aforementioned scenario is representative of the crust of Hole 1256D, the ~100 m accumulation of pillows in Hole 1256D may be explained by the axial slope covered by pillow lavas as observed by *Shinkai 6500* dives.

5.3. EPR Lava Deposition History in Hole 1256D

[26] The volcanostratigraphy model, from the base to the top of the extrusive section, allows to recon-

struct the upper ocean crust constructional processes of the EPR, as represented by evolution of lava deposition from on-axis to off-axis environments. We use the observations from the EPR 14°S and EPR 9°N spreading centers [*Escartín et al.*, 2007; *Umino et al.*, 2008a, 2008b] and the axial slope topography and Hole 1256D half spreading rate [*Wilson et al.*, 2003] to build a time-distance reference frame. We assume the location of the axial slope and the base of the slope to be at ~1000 to 2000 m and 2000–3000 m from the ridge axis, respectively. Based on our scenario from section 5.2, this time-distance reference frame places the 100 m pillow interval at the axial slope. This 100 m pillow-dominated interval subdivides the extrusive sequence into two parts: lavas below this interval that were deposited before the crust moved and reached the axial slope, and lavas above this interval were deposited after the crust passed and moved away from the axial slope.

[27] We propose five constructional stages (A–E). In stage A, the intrusive-extrusive boundary is marked by the lowermost fragmented flow at the ridge axis atop the sheeted dike complex (1064 mbsf, stage A in Figure 8). In stage B, thick layers of massive flows and breccias directly atop this boundary are attributed to the accumulation of high eruption rate flows and collapsed pits that may a result of drain back or drainage of lavas (stage B in Figure 8) [*Gregg and Chadwick*, 1996; *Sims et al.*, 2003]. Isolated dike margins are observed as shallow as 825 mbsf within this interval, indicating that these dikes branched out from the melt lens following low-pressured pathways (fractures) associating with or without major dike intrusion events at the eruption center on the axis. Layers of fragmented flows, thinner flows, and breccias from 850 to 950 mbsf might have been tectonized by faulting and/or collapsed flow lobes around the axial summit (also see section 4.1 and Table 2). In stage C, when lateral translation of Hole 1256D by seafloor spreading had placed the hole at the axial slope, sheet flows as well as elongated pillows that dribbled down the slope accumulated. Localized pillows between 710–800 mbsf are formed at the axial slope (1000–2000 m from the ridge axis) (stage C in Figure 8). In stage D, the overlying extrusive rocks, predominantly a sequence of thick layers of massive flows, fragmented flows, and breccias (350–710 mbsf-C), presumably formed within 2000–3000 m from the ridge axis where long lava flows are terminated and ponded by inward facing faults [*Escartín et al.*, 2007] (stage D in Figure 8). This location estimate is augmented by the presence of inflation cracks (subvertical veins filled by hyaloclastite; Core 1256D-21R-1, 85–140 cm at 397.6–398.2 mbsf-C) and seal zone (recrystallized fine-grained chilled margins of flow lobes; Core 1256D-37R-2, 12–15 cm at 501.7 mbsf-C) of coalesced flow lobes [*Wilson et al.*, 2003] that characterize inflated lobate sheets. Stage E is the construction of off-axis ponded lava section (stage E in Figure 8).

[28] Our correlation suggests that the crust moved from the ridge axis to the bottom of the axial slope over a period of 10–20 kyr (~2 km), during which time nearly 50% of the extrusive sequence in the hole is constructed (stage C in Figure 8) and nearly 100% of the layer 2A construction within ~3000 m of the ridge axis, except for the contribution from late stage off-axis eruptions that formed the lava pond (stage E in Figure 8). This construction rate is similar to a widely accepted geophysical conceptual model [e.g., *Hooft et al.*, 1996] and the observations from the more recent near bottom surveys around the EPR 9°N [*Escartín et al.*, 2007]. Furthermore, the depth to the to of the gabbro section in Hole 1256D supports our construction rates in terms of the relationship between the thickness of layer 2A and the depth to the axial melt lens. A strong positive correlation is observed between the thickness of layer 2A and the depth to the magma lens [*Blacic et al.*, 2004], in which a layer 2A thickness (the weight of the overlying lavas on a ridge axis) and the depth to the axial magma chamber (magma lens pressure that is required to feed magma to the surface) have linear relationship [*Buck et al.*, 1997; *Blacic et al.*, 2004, Figure 11]. Using this observation, the depth to the drilled first gabbro layer, 1157 m subseafloor [*Wilson et al.*, 2006], yields approximately 200 ± 40 m for the thickness of on-axis layer 2A, variations of which depend on isostasy models. This layer 2A thickness is consistent with the thickness of on-axis extrusive lavas in Hole

Figure 8. Hole 1256D flow stratigraphy (stages A–E) and lava deposition history models. For the flow stratigraphy model, we used logging depth (mbsf-L). Distance and age scales for lava deposition history are located atop (horizontal axis) the stratigraphy. The construction rates are indicated as partially filled in circles located atop the stratigraphy. Typical axial morphology (in boxes) and proportion of how much of layer 2 was formed (circles) are also shown along the scales. Each of the stages shows approximate time and location for the formation of a portion of extrusive section in Hole 1256D.

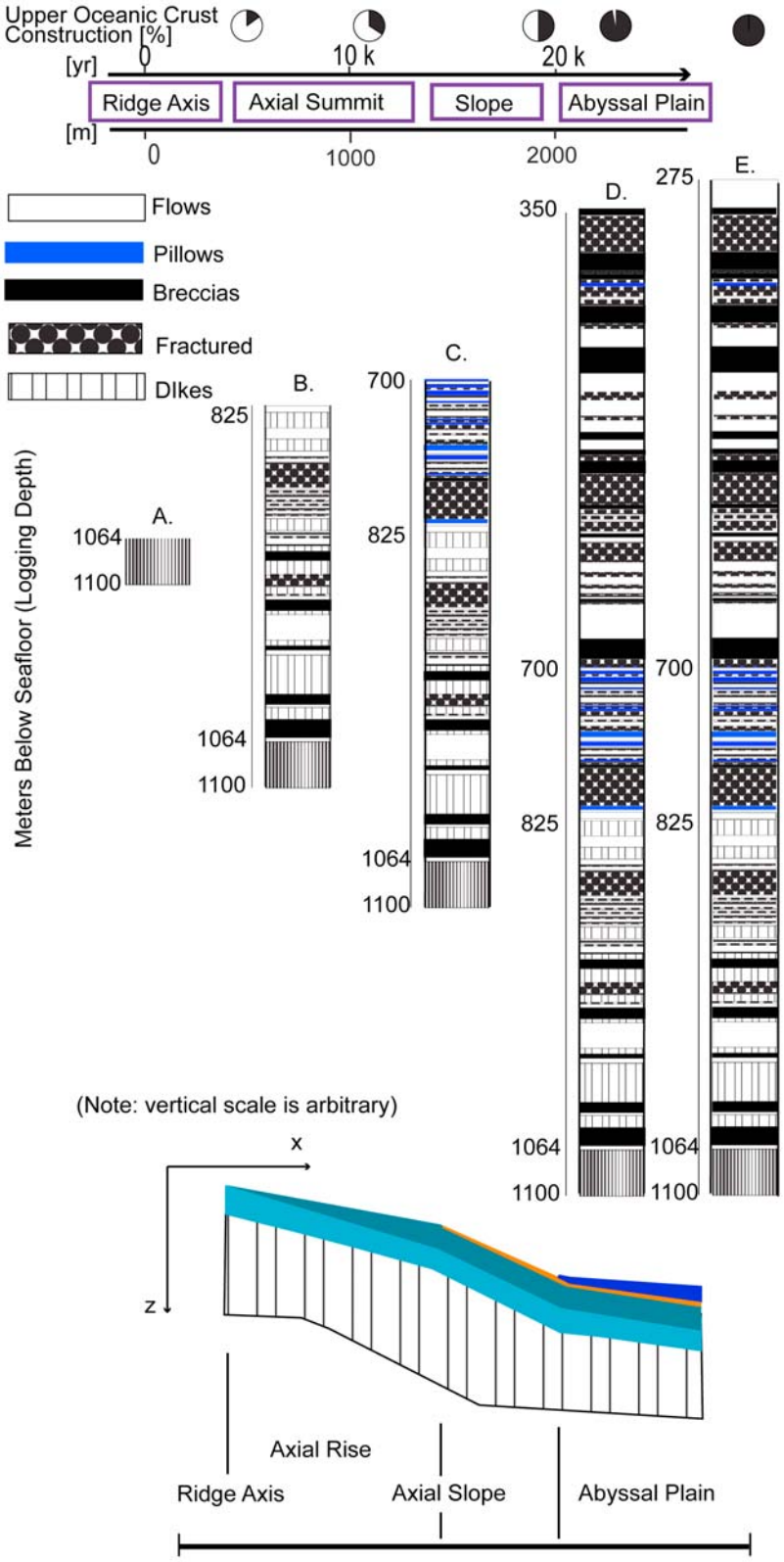
Upper Oceanic Crust Construction [%]
[yr]
0
10 k
20 k
Ridge Axis
Axial Summit
Slope
Abyssal Plain
[m]
0
1000
2000
Flows
Pillows
Breccias
Fractured
Dlkes
Meters Below Seafloor (Logging Depth)
A.
B.
C.
D.
E.
1064
1100
825
700
350
275
(Note: vertical scale is arbitrary)
x
z
Axial Rise
Ridge Axis
Axial Slope
Abyssal Plain

Figure 8

1256D during lava deposition stages A and B, suggesting the predicted upper crust construction rate from this study is consistent to the deposition history of Hole 1256D.

6. Conclusions

[29] We draw the following conclusions from this study.

[30] 1. The electrofacies analysis principally based on FMS images suggests that Hole 1256D crust (250–1425 mbsf) can be classified into ten electrofacies: massive flows, massive off-axis ponded lava, fractured massive flows, fragmented flows, sheet flows or thick pillows, pillows, breccias, isolated dikes, dikes in a sheeted dike complex, and gabbros. These 10 electrofacies can be clustered into 4 principal families of flow morphology. The resulting flow stratigraphy corresponds to lava flow morphology and deposition styles observed on the EPR: sheet flows, pillows, breccias, and dikes.

[31] 2. The observations from two *Shinkai 6500* dives on the EPR 14°S show that the formation of pillow lavas is primarily controlled by changes in slope angles (gradient) of local topography. The correlation between lava flow types and slope angles indicates that a slope angle of 5° is the threshold, beyond which pillows are formed. If the lava distribution observed at the EPR 14°S is applicable to 1256D crust, the flow stratigraphy can be used to recreate the upper oceanic crust construction process. The spatial reference frame for modeling the lava deposition history in Hole 1256D is obtained from both EPR 14°S and 9°N axial morphology.

[32] 3. By integrating the flow stratigraphy in Hole 1256D with the EPR 14°S observations, we propose a scenario of Assuming paleospreading rate was constant with 50% of the extrusive rocks in Hole 1256D crust were formed within ~2 km of the ridge axis while nearly all of the remaining extrusive section likely formed within ~3 km of the ridge axis. This construction progress rate is consistent to a widely accepted conceptual model of *Hooft et al.* [1996]. Furthermore, the observed correlation between on-axis layer 2A thickness and the depth to the axial magma chamber also supports the idea that the depth to the drilled gabbro in Hole 1256D results in our prediction of upper crustal construction rates in Hole 1256D. Our lava deposition history model is the first to use drilled hole volcanic stratigraphy to interpret lava flow architecture and thereby reveal upper oceanic construction processes.

Acknowledgments

[33] We thank the editors of G-Cubed, V. Salters and D. Teagle, and two anonymous reviewers for improving this manuscript. M.T. thanks S. A. Soule for access to his EPR data and M. A. Tivey for improving the language of this manuscript. S.U. was supported by the Center of Deep Earth Exploration (CDEX) for travel fares and by Monbusho grant-in-aid for research 18540472. Dive transects were done during the NIR-AI-KANAI cruise (YK04–07) using the R/V *Yokosuka* and *Shinkai 6500* submersible of Japan Agency for Marine-Earth Science and Technology (JAMSTEC). This research used data provided by the Ocean Drilling Program and the Integrated Ocean Drilling Program.

References

Alt, J. C. (1994), A sulfur isotopic profile through the Troodos ophiolite, Cyprus: Primary composition and the effects of seawater hydrothermal alteration, *Geochim. Cosmochim. Acta*, *58*, 1825–1840, doi:10.1016/0016-7037(94)90539-8.

Alt, J. C., et al. (1993), *Proceedings of the Ocean Drilling Program, Initial Reports*, vol. 148, Ocean Drill. Program, College Station, Tex.

Alt, J. C., et al. (1996), Hydrothermal alteration of a section of upper oceanic crust in the eastern equatorial Pacific: A synthesis of results from Site 504 (DSDP Legs 69, 70 and 83, and ODP Legs 111, 137, 140, and 148), *Proc. Ocean Drill. Program Sci. Results*, *148*, 417–434.

Auzende, J.-M., et al. (1996), Recent tectonic, magmatic, and hydrothermal activity on the East Pacific Rise between 17°S and 19°S: Submersible observations, *J. Geophys. Res.*, *101*, 17,995–18,010, doi:10.1029/96JB01209.

Ballard, R. D., and J. G. Moore (1977), *Photographic Atlas of the Mid Atlantic Ridge Rift Valley*, 114 pp., Springer, New York.

Batiza, R., and J. D. L. White (2000), Submarine lavas and hyaloclastite, in *Encyclopedia of Volcanoes*, edited by H. Sigurdsson et al., pp. 361–381, Academic, San Diego, Calif.

Bazin, S., et al. (2001), Three-dimensional shallow crustal emplacement at the 9°03′N overlapping spreading center on the East Pacific Rise: Correlations between magnetization and tomographic images, *J. Geophys. Res.*, *106*, 16,101–16,117.

Bednarz, U., and H.-U. Schumincke (1989), Mass transfer during sub-seafloor alteration of the upper Troodos crust, *Contrib. Mineral. Petrol.*, *102*, 93–101, doi:10.1007/BF01160193.

Blacic, T. M., G. Ito, J. P. Canales, R. S. Detrick, and J. Sinton (2004), Constructing the crust along the Galapagos Spreading Center 91.3°–95.5°W: Correlation of seismic layer 2A with axial magma lens and topographic characteristics, *J. Geophys. Res.*, *109*, B10310, doi:10.1029/2004JB003066.

Bohnenstiehl, D. R., and S. M. Carbotte (2001), Faulting patterns near 19°30′S on the East Pacific Rise: Fault formation and growth at a superfast spreading center, *Geochem. Geophys. Geosyst.*, *2*(9), 1056, doi:10.1029/2001GC000156.

Bonatti, E., and C. G. A. Harrison (1988), Eruption styles of basalt in oceanic spreading ridges and seamounts: Effect of magma temperature and viscosity, *J. Geophys. Res.*, *93*, 2967–2980, doi:10.1029/JB093iB04p02967.

Buck, W. R., S. M. Carbotte, and C. Mutter (1997), Controls on extrusion at mid-ocean ridges, *Geology*, *25*, 935–938.

Casey, J. F., J. F. Dewey, P. J. Fox, J. A. Karson, and E. Rosencrantz (1981), Heterogeneous nature of oceanic crust and upper mantle: A perspective from the Bay of Islands Ophiolite Complex, in *The Sea*, vol. 7, *The Oceanic Lithosphere*, edited by C. E. Emiliani, pp. 305–338, John Wiley, New York.

Christeson, G. L., K. D. Mclntosh, and J. A. Karson (2007), Inconsistent correlation of seismic layer 2a and lava layer thickness in oceanic crust, *Nature*, *445*, 418–421, doi:10.1038/nature05517.

Coleman, R. G. (1977), *Ophiolites—Ancient Oceanic Lithosphere?*, 299 pp., Springer, Berlin.

Cormier, M.-H., W. B. F. Ryan, A. K. Shah, W. Jin, A. M. Bradley, and D. R. Yoerger (2003), Waxing and waning volcanism along the East Pacific Rise on a millennium time scale, *Geology*, *31*, 633–636, doi:10.1130/0091-7613(2003)031<0633:WAWVAT>2.0.CO;2.

Crispini, L., P. Tartarotti, and S. Umino (2006), Microstructural features of a subaqueous lava from basaltic crust off the East Pacific Rise (ODP Site 1256, Cocos Plate), *Ofioliti*, *31*, 117–127.

Dilek, Y., E. M. Moores, and H. Furnes (1998), Structure of modern oceanic crust and ophiolites and implications for faulting and magmatism at oceanic spreading centers, in *Faulting and Magmatism at Mid-Ocean Ridges*, *Geophys. Monogr. Ser.*, vol. 106, edited by W. R. Buck et al., pp. 153–176, AGU, Washington, D. C.

Embley, R. W., J. E. Lupton, G. Massoth, T. Urabe, V. Tunnicliffe, D. A. Butterfield, T. Shibata, O. Okano, M. Knoshita, and K. Fujioka (1998), Geological, chemical, and biological evidence for recent volcanism at 17.5°S: East Pacific Rise, *Earth Planet. Sci. Lett.*, *163*, 131–147, doi:10.1016/S0012-821X(98)00181-2.

Engels, J. L., M. H. Edwards, D. J. Fornari, M. R. Perfit, and J. R. Cann (2003), A new model for submarine volcanic collapse formation, *Geochem. Geophys. Geosyst.*, *4*(9), 1077, doi:10.1029/2002GC000483.

Escartín, J., S. A. Soule, D. J. Fornari, M. A. Tivey, H. Schouten, and M. R. Perfit (2007), Interplay between faults and lava flows in construction of the upper oceanic crust: The East Pacific Rise crest 9°25′–9°58′N, *Geochem. Geophys. Geosyst.*, *8*, Q06005, doi:10.1029/2006GC001399.

Ferrini, V. L., D. J. Fornari, T. M. Shank, J. C. Kinsey, M. A. Tivey, S. A. Soule, S. M. Carbotte, L. L. Whitcomb, D. Yoerger, and J. Howland (2007), Submeter bathymetric mapping of volcanic and hydrothermal features on the East Pacific Rise crest at 9°50′N, *Geochem. Geophys. Geosyst.*, *8*, Q01006, doi:10.1029/2006GC001333.

Fisher, N. I. T. L., and B. J. J. Embleton (1987), *Statistical Analysis of Spherical Data*, 329 pp., Cambridge Univ. Press, Cambridge, U. K.

Fornari, D. J. (1986), Submarine lava tubes and channels, *Bull. Volcanol.*, *48*, 291–298, doi:10.1007/BF01081757.

Fornari, D. J., A. Malahoff, and B. C. Heezen (1979), Visual observations of the volcanic micromorphology of Tortuga, Lorraine and Tutu seamounts; and petrology and chemistry of ridge and seamount features in and around the Panama Basin, *Mar. Geol.*, *31*, 1–30, doi:10.1016/0025-3227(79)90054-9.

Fornari, D. J., R. M. Haymon, M. R. Perfit, T. K. P. Gregg, and M. H. Edwards (1998), Geological characteristics and evolution of the axial zone on fast spreading mid-ocean ridges: Formation of an axial summit trough along the East Pacific Rise, 9°–10°N, *J. Geophys. Res.*, *103*, 9827–9855, doi:10.1029/98JB00028.

Fornari, D., et al. (2004), Submarine lava flow emplacement at the East Pacific Rise 9°50N: Implications for uppermost ocean crust stratigraphy and hydrothermal fluid circulation, in *Mid-Ocean Ridges: Hydrothermal Interactions Between the Lithosphere and Oceans*, *Geophys. Monogr. Ser.*, vol. 148, edited by C. R. German, J. Lin, and L. M. Parson, pp. 187–218, AGU, Washington, D. C.

Francheteau, J., and R. D. Ballard (1983), The East Pacific Rise near 21°N, 13°N, and 20°S: Inferences for along-strike variability of axial processes of the Mid-Ocean Ridge, *Earth Planet. Sci. Lett.*, *64*, 93–116, doi:10.1016/0012-821X(83)90055-9.

Geshi, N., S. Umino, H. Kumagai, J. M. Sinton, S. M. White, K. Kishimoto, and T. W. Hilde (2007), Discrete plumbing systems and heterogeneous magma sources of a 24 km^3 off-axis lava field on the western flank of East Pacific Rise, 14°S, *Earth Planet. Sci. Lett.*, *258*, 61–72, doi:10.1016/j.epsl.2007.03.019.

Gilbert, L. A., and A. Burke (2008), Depth-shifting cores incompletely recovered from the upper oceanic crust, IODP Hole 1256D, *Geochem. Geophys. Geosyst.*, *9*, Q08O11, doi:10.1029/2008GC002010.

Gillis, K. M., and K. Sapp (1997), Distribution of porosity in a section of upper oceanic crust exposed in the Troodos Ophiolite, *J. Geophys. Res.*, *102*, 10,133–10,149, doi:10.1029/96JB03909.

Giordano, D., J. K. Russell, and D. B. Dingwell (2008), Viscosity of magmatic liquids: A model, *Earth Planet. Sci. Lett.*, *271*, 123–134, doi:10.1016/j.epsl.2008.03.038.

Gregg, T. K. P., and W. W. Chadwick (1996), Submarine lava-flow inflation: A model for the formation of lava pillars, *Geology*, *24*, 981–984, doi:10.1130/0091-7613(1996)024<0981:SLFIAM>2.3.CO;2.

Gregg, T. K. P., and J. H. Fink (1995), Quantification of submarine lava-flow morphology through analog experiments, *Geology*, *23*, 73–76, doi:10.1130/0091-7613(1995)023<0073:QOSLFM>2.3.CO;2.

Gregg, T. K. P., and D. K. Smith (2003), Volcanic investigations of the Puna Ridge, Hawai'i: Relations of lava flow morphologies and underlying slopes, *J. Volcanol. Geotherm. Res.*, *126*, 63–77.

Griffiths, R. W. (2000), The dynamics of lava flows, *Annu. Rev. Fluid Mech.*, *32*, 477–518, doi:10.1146/annurev.fluid.32.1.477.

Haymon, R. M., et al. (1993), Volcanic eruption of the mid-ocean ridge along the East Pacific Rise crest at 9°45–52′N: Direct submersible observations of seafloor phenomena associated with an eruption event in April, 1991, *Earth Planet. Sci. Lett.*, *119*, 85–101, doi:10.1016/0012-821X(93)90008-W.

Hooft, E. E. E., H. Schouten, and R. S. Detrick (1996), Constraining crustal emplacement processes from the variation in seismic layer 2A thickness at the East Pacific Rise, *Earth Planet. Sci. Lett.*, *142*, 289–309, doi:10.1016/0012-821X(96)00101-X.

Karson, J. A., et al. (2002), Structure of uppermost fast-spread oceanic crust exposed at the Hess Deep Rift: Implications for subaxial processes at the East Pacific Rise, *Geochem. Geophys. Geosyst.*, *3*(1), 1002, doi:10.1029/2001GC000155.

Koepke, J., J. Berndt, S. T. Feig, and F. Holtz (2007), The formation of SiO_2-rich melts within the deep oceanic crust by hydrous partial melting of gabbros, *Contrib. Mineral. Petrol.*, *153*, 67–84.

Kurras, G. J., D. J. Fornari, M. H. Edwards, M. R. Perfit, and M. C. Smith (2000), Volcanic morphology of the East Pacific Rise Crest 9°49–52′: Implications for volcanic emplacement processes at fast-spreading mid-ocean ridges, *Mar. Geophys. Res.*, *21*, 23–41, doi:10.1023/A:1004792202764.

Macdonald, K. C., P. J. Fox, R. T. Alexander, R. Pockalny, and P. Gente (1996), Volcanic growth faults and the origin of Pacific abyssal hills, *Nature*, *380*, 125–129, doi:10.1038/380125a0.

Moores, E. M., and E. D. Jackson (1974), Ophiolites and oceanic crusts, *Nature*, *250*, 136–139, doi:10.1038/250136a0.

Moores, E. M., and F. J. Vine (1971), The Troodos Massif, Cyprus and other ophiolites and oceanic crust: Evaluations and implications, *Philos. Trans. R. Soc. London*, *A268*, 443–466.

Nicolas, A. (1995), *The Mid-Oceanic Ridges*, 200 pp., Springer, Berlin.

Perfit, M. R., J. R. Cann, D. J. Fornari, J. Engles, D. K. Smith, W. Ian Ridley, and M. H. Edwards (2003), Interaction of sea water and lava during submarine eruptions at mid-ocean ridges, *Nature*, *426*, 62–65, doi:10.1038/nature02032.

Pezard, P. A. (1990), Electrical properties of mid-ocean ridge basalt and implications for the structure of the upper oceanic crust in Hole 504B, *J. Geophys. Res.*, *95*, 9237–9264, doi:10.1029/JB095iB06p09237.

Putirka, K. (1999), Clinopyroxene + liquid equilibria to 100 kbar and 2450 K, *Contrib. Mineral. Petrol.*, *135*, 151–163.

Rautenschlein, M. (1987), Geology and geochemistry of the Akaki volcanics, Cyprus, Ph.D. dissertation, 222 pp., Ruhr-Univ. Bochum, Bochum, Germany.

Scheirer, D. S., D. J. Fornari, S. E. Humphris, and S. Lerner (2000), High-resolution seafloor mapping using the DSL-120 sonar system: Quantitative assessment of sidescan and phase-bathymetry data from the Lucky Strike segment of the Mid-Atlantic Ridge, *Mar. Geophys. Res.*, *21*, 121–142, doi:10.1023/A:1004701429848.

Schmincke, H.-U., P. T. Robinson, W. Ohnmacht, and M. F. J. Flower (1978), Basaltic hyaloclastites from holes 396B, DSDP Leg 46, *Initial Rep. Deep Sea Drill. Proj.*, *46*, 341–355.

Schouten, H., and C. R. Denham (1979), Modeling the oceanic magnetic source layer, in *Deep Drilling Results in the Atlantic Ocean: Ocean Crust*, *Maurice Ewing Ser.*, vol. 2, edited by M. Talwani et al., pp. 151–159, AGU, Washington, D. C.

Sempéré, J., and K. C. Macdonald (1986), Deep-tow studies of the overlapping spreading centers at 9°03′N on the East Pacific Rise, *Tectonics*, *5*, 881–900, doi:10.1029/TC005i006p00881.

Sims, K. W. W., et al. (2003), Aberrant youth: Chemical and isotopic constraints on the origin of off-axis lavas from the East Pacific Rise, 9°–10°N, *Geochem. Geophys. Geosyst.*, *4*(10), 8621, doi:10.1029/2002GC000443.

Sinton, J., E. Bergmanis, K. Rubin, R. Batiza, T. K. P. Gregg, K. Grönvold, K. C. Macdonald, and S. M. White (2002), Volcanic eruptions on mid-ocean ridges: New evidence from the superfast spreading East Pacific Rise, 17°–19°S, *J. Geophys. Res.*, *107*(B6), 2115, doi:10.1029/2000JB000090.

Smith, W. H., and D. T. Sandwell (1997), Global seafloor topography from satellite altimetry and ship depth soundings, *Science*, *227*, 1956–1962.

Soule, S. A., K. V. Cashman, and J. P. Kauahikaua (2004), Examining flow emplacement through the surface morphology of three rapidly emplaced, solidified lava flows, Kilauea Volcano, Hawai'i, *Bull. Volcanol.*, *66*, 1–14.

Soule, S. A., D. J. Fornari, M. R. Perfit, M. A. Tivey, W. I. Ridley, and H. Schouten (2005), Channelized lava flows at the East Pacific Rise crest 9°–10°N: The importance of off-axis lava transport in developing the architecture of young oceanic crust, *Geochem. Geophys. Geosyst.*, *6*, Q08005, doi:10.1029/2005GC000912.

Soule, S. A., D. J. Fornari, M. R. Perfit, and K. H. Rubin (2007), New insights into mid-ocean ridge volcanic processes from the 2005–2006 eruption of the East Pacific Rise, 9°46′N–9°56′N, *Geology*, *35*, 1079–1082, doi:10.1130/G23924A.1.

Soule, S. A., J. Escartín, and D. J. Fornari (2009), A record of eruption and intrusion at a fast spreading ridge axis: Axial summit trough of the East Pacific Rise at 9–10°N, *Geochem. Geophys. Geosyst.*, *10*, Q10T07, doi:10.1029/2008GC002354.

Stakes, D. S., M. R. Perfit, M. A. Tivey, D. W. Caress, T. M. Ramirez, and N. Maher (2006), The Cleft revealed: Geologic, magnetic, and morphologic evidence for construction of upper oceanic crust along the southern Juan de Fuca Ridge, *Geochem. Geophys. Geosyst.*, *7*, Q04003, doi:10.1029/2005GC001038.

Teagle, D. A. H., J. C. Alt, S. Umino, S. Miyashita, N. R. Banerjee, D. S. Wilson, and the Expedition 309/312 Scientists (2006), *Proceedings of the Integrated Ocean Drilling Program*, vol. 309/312, pp. 1–27, doi:10.2204/iodp.proc.309312.101.2006, Integrated Ocean Drill. Program, Washington, D. C.

Tominaga, M., D. A. H. Teagle, J. C. Alt, and S. Umino (2009), Determination of the volcanostratigraphy of oceanic crust formed at superfast spreading ridge: Electrofacies analyses of ODP/IODP Hole 1256D, *Geochem. Geophys. Geosyst.*, *10*, Q01003, doi:10.1029/2008GC002143.

Umino, S., P. W. Lipman, and S. Obata (2000), Subaqueous lava flow lobes, observed on ROV *KAIKO* dives off Hawaii, *Geology*, *28*, 503–506, doi:10.1130/0091-7613(2000)28<503:SLFLOO>2.0.CO;2.

Umino, S., S. Obata, P. Lipman, J. R. Smith, T. Shibata, J. Naka, and F. Trusdell (2002), Emplacement and inflation structures of submarine and subaerial pahoehoe lavas from Hawaii, in *Hawaiian Volcanoes: Deep Underwater Perspectives*, *Geophys. Monogr. Ser.*, vol. 128, edited by E. Takahashi et al., pp. 85–101, AGU, Washington, D. C.

Umino, S., K. Kisimoto, T. W. C. Hilde, N. Geshi, S. M. White, H. Kumagai, and J. M. Sinton (2008a), Slope control of the submarine lava morphology revealed by the transect across the southern East Pacific Rise, paper presented at 5th Annual Meeting, Asia Oceania Geosci. Soc., Busan, South Korea.

Umino, S., K. Kisimoto, T. W. C. Hilde, N. Geshi, H. Kumagai, S. M. White, and J. M. Sinton (2008b), Slope control of the submarine lava morphology revealed by the transect across the southern East Pacific Rise at 14°S, paper presented at Autumn Meeting, Volcanol. Soc. Jpn., Morioka, Japan.

White, S. M., K. C. Macdonald, and R. M. Haymon (2000), Basaltic lava domes, lava lakes, and volcanic segmentation on the southern East Pacific Rise, *J. Geophys. Res.*, *105*, 23,519–23,536, doi:10.1029/2000JB900248.

White, S. M., R. M. Haymon, D. J. Fornari, M. R. Perfit, and K. C. Macdonald (2002), Correlation between volcanic and tectonic segmentation of fast-spreading ridges: Evidence from volcanic structures and lava flow morphology on the

East Pacific Rise at 9°–10°N, *J. Geophys. Res.*, *107*(B8), 2173, doi:10.1029/2001JB000571.

White, S. M., J. L. Mason, K. C. Macdonald, M. R. Perfit, V. D. Wanless, and E. M. Klein (2009), Significance of widespread low effusion rate eruptions over the past two million years for delivery of magma to the overlapping spreading centers at 9°N East Pacific Rise, *Earth Planet. Sci. Lett.*, *280*, 175–184.

Wilson, D. S., D. A. H. Teagle, and G. D. Acton (2003), *Proceedings of the Ocean Drilling Program, Initial Report* [online], vol. 206, Ocean Drill. Program, College Station, Tex. (Available at http://www-odp.tamu.edu/publications/206_IR/206ir.htm)

Wilson, D. S., et al. (2006), Drilling to gabbro in intact ocean crust, *Science*, *312*, 1016–1020, doi:10.1126/science.1126090.

Wright, D. J., R. M. Haymon, and D. J. Fornari (1995), Crustal fissuring and its relationship to magnetic and hydrothermal processes on the East Pacific Rise crest (9°12′ to 54′N), *J. Geophys. Res.*, *100*, 6097–6120, doi:10.1029/94JB02876.

Yamagishi, H. (1994), *Subaqueous Volcanic Rocks: Atlas and Glossary*, 195 pp., Hokkaido Univ. Press, Sapporo, Japan.